Image formation in CARS and SRS: effect of an inhomogeneous nonresonant background medium

K. I. Popov,[1,*] A. F. Pegoraro,[2,3] A. Stolow,[1,2,3] and L. Ramunno[1]

[1]*Department of Physics, University of Ottawa, Ottawa, Ontario K1N 6N5, Canada*

[2]*Steacie Institute for Molecular Sciences, National Research Council of Canada, Ottawa, Ontario, K1A 0R6 Canada*

[3]*Department of Physics, Queen's University, Kingston, Ontario, K7L 3N6 Canada*

**Corresponding author: kpopov@uottawa.ca*

Received October 24, 2011; revised December 15, 2011; accepted December 16, 2011;
posted December 16, 2011 (Doc. ID 156902); published February 6, 2012

We investigate the role of a spatially inhomogenous nonresonant background medium on several Raman-based imaging modalities. In particular, we consider a small resonant bead submerged in a spatially heterogeneous nonresonant $\chi^{(3)}$ background. Using detailed 3D electrodynamic simulations, we compare coherent anti-Stokes Raman scattering (CARS), frequency-modulated CARS, amplitude-modulated stimulated Raman scattering (SRS), and frequency-modulated SRS. We find that only FM-SRS is background-free. © 2012 Optical Society of America

OCIS codes: 180.4315, 180.5655.

Raman-based nonlinear optical microscopies permit label-free, chemical-specific, video-rate imaging in a broad range of applications, notably the nondestructive *in vivo* imaging of biological tissues and cells. Over the past decade, there have been many advancements in CARS, and it has seen much success, for example, as a tool for understanding lipid biology in real time [1,2]. More recently, video-rate acquisition has also been demonstrated with SRS [3] microscopy. Because of the inherent linear scaling of SRS signals with number of oscillators in the focal volume, this method holds promise for the imaging much lower-density objects, potentially giving a unique window into the visualization of biological processes involving proteins. Currently, as few as $\sim 3 \times 10^5$ oscillators can be detected in the focal volume by SRS, with a further room to increase this sensitivity [4].

One inherent drawback of CARS is the existence of the nonresonant background. The CARS signal is generated in a third-order coherent nonlinear four-wave mixing process between excitation laser pulses. When the laser pulse beat-wave frequency is resonant with a vibrational frequency of interest within the sample of sufficient density, a strong CARS signal is generated. However, even if the third-order susceptibility $\chi^{(3)}$ in the sample does not possess a resonance, a certain amount of nonresonant CARS signal will also be generated. If the concentration of the resonant species is relatively small, the nonresonant signal can overwhelm the resonant one, reducing the image contrast considerably. The presence of the nonresonant background signal has also been shown to result in both spectral [1] and spatial [5] distortions in the image.

There have been several methods proposed to reduce the nonresonant background signal [1,6,7], one of the most successful being frequency-modulated CARS (FM-CARS) [8]. Here, either the pump or Stokes inputs of the laser pulse are frequency-modulated so that their difference is modulated on and off the vibrational resonance. This results in a signal at the anti-Stokes frequency that is modulated between two values: one corresponding to purely nonresonant interaction, and the other to both the resonant and nonresonant interactions. The difference between these two signals effectively removes the average background contribution, and gives much improved image contrast. However, we show that FM-CARS does not directly address the image distortions caused by interference with the background signal.

SRS microscopy is based on detecting either depletion of the pump or gain in the Stokes pulse via the stimulated Raman scattering process. There have been two proposed methods for measuring the SRS signal, one based on the modulation of the frequency shift between the pump and Stokes (FM-SRS, [9]) and the other based on the modulation of the pump or Stokes source amplitude (AM-SRS, [3,4,10,11]). SRS is an incoherent process which, unlike CARS, does not rely on the coherent generation of a new frequency and is not expected to suffer from contamination from a nonresonant signal.

In this Letter, we show that of all the coherent Raman-scattering-based imaging modalities considered, only FM-SRS appears background-free. We analyze the forward-detected signal in each of the techniques mentioned above (i.e., CARS, FM-CARS, FM-SRS, and AM-SRS) and, in particular, examine the effects of spatial inhomogeneities in the nonresonant background medium on image formation. Realistic samples are very heterogeneous and therefore understanding how heterogeneity affects the image formation is critical for its proper interpretation. The system modeled here is composed of a subwavelength-sized Raman-active spherical bead in the presence of background material. We consider three situations: (1) the background medium is uniform throughout the entire space; (2) the background occupies only the semispace before the focal plane where it is spatially homogeneous; and (3) the background occupies only the semispace after the focal plane (where it is also spatially homogeneous). The last two scenarios represent the simplest cases of a spatially nonuniform nonresonant background medium. The three cases described above are depicted in Fig. 1.

In our analysis, we used numerical simulation tools previously employed in Ref. [5]. We performed 3D

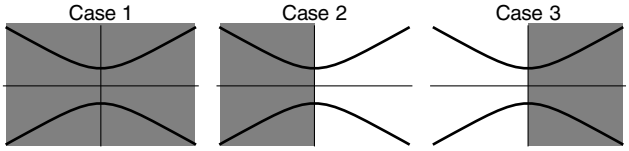

Fig. 1. Schematic draft of the three cases considered in the text. The thick lines represent the focused pulse shape and the shaded region indicates the presence of the nonresonant $\chi^{(3)} \neq 0$. The laser pulse propagates from left to right in the figures.

finite-difference time-domain (FDTD) simulations of the interaction between these objects and the laser source. The scattered light is then collected in the far field in the forward direction where its intensity is integrated over a solid angle corresponding to a condenser lens with NA $= 0.6$. The laser lens has NA $= 1.1$. We assumed a value of $\chi^{(3)} = 2 \times 10^{-14}$esu for the background medium, corresponding to the $\chi^{(3)}$ of water [12]. The resonant $\chi^{(3)}$ was chosen such that the produced resonant bulk CARS signal is ~50 times larger than the nonresonant one (cf. [13]). The radius of the bead used was $0.4\,\mu$m, the pump wavelength was $0.8\,\mu$m (measured in vacuum), the resonant Stokes wavelength was $1.042\,\mu$m, and the off-resonant (used in the frequency modulation) Stokes wavelength was $1.087\,\mu$m. In this way, the off-resonant Stokes pulse was displaced from the central resonance by four Raman resonance widths. The laser source intensity was of the order of 10^9 W/cm^2. The refraction index in the entire space was assumed $n_0 = 1.33$, even in the simulations with a spatially nonuniform background, so as to emphasize nonlinear effects on the image formation process. The refraction index in the bead was assumed to be 1.5.

In our simulations, the Raman bead was placed on the laser axis, and the CARS or SRS signals were measured as functions of the bead center position x_c relative to the laser focus. The results are given in Fig. 2. The CARS signal dependence on the bead position is shown in Fig. 2(a). This signal pattern was analyzed in detail in Ref. [5] for the case of a spatially uniform background (case 1, solid line). All the three plots in Fig. 2(a), corresponding to the three cases from Fig. 1 reveal characteristic features caused by interference between the resonant and nonresonant signals: a shadow when the bead is located before the focus, and a peak when the bead is located after the focus. When only half of the space is occupied by the nonresonant medium, the nonresonant signal intensity decreases while overall contrast increases since the resonant signal is unchanged. Because of the Gouy phase shift, the phases of the nonresonant signal generated by the two different half-spaces are different, resulting in different interference patterns. For this reason, the thick dashed and dotted curves in Fig. 2(a) do not coincide.

To model the FM-CARS signal, we have performed two sets of simulations: one with the Stokes frequency shifted from the pump by exactly the Raman resonant frequency, and the other with a detuned Stokes. The difference between the two anti-Stokes intensities produced the FM-CARS signals shown in Fig. 2(b). We see that the background signal in the absence of Raman scatterers is greatly suppressed (although it did not completely vanish in our simulations since we assumed the tuned and detuned Stokes to be of equal intensity and focused by the same optics, i.e., their actual energy was slightly different). However, the FM-CARS signals still contain spatial distortions, manifested by the peak shift and appearance of a negative FM-CARS signal at negative x_c. This phenomenon is caused by the fact that the interference between the resonant and nonresonant signals from the on-resonance pulses is not equal to the sum of intensities of these two signals.

The simulations results for AM-SRS are shown in Fig. 2(c). The curves represent the difference between forward-measured pump signals in two situations: when the Stokes is on, and when it is off. Since SRS is an incoherent process, one would expect the modulation of the pump depletion to be caused entirely by the presence of resonant scatterers. Indeed, as indicated by the solid lines in Fig. 2(c), the AM-SRS seems background-free when the nonresonant background medium is spatially homogeneous. However, in the cases of the spatially inhomogeneous backgrounds, we observe a strong background signal, with an amplitude that is comparable to the resonant signal itself. This background signal is observable (and, in fact, can be overwhelming) for a wide range of $\chi^{(3)}$ values of the background medium and depends on the parameters of the microscope signal collecting optics, as illustrated in Fig. 3. It follows that for the fixed sample geometry and condenser lens NA, the magnitude of the nonresonant signal in AM-SRS is linearly dependent on $\chi^{(3)}$. As the NA of the condenser NA grows, the background signal level decreases and approaches a finite limit, for the given $\chi^{(3)}$.

We can understand this behavior by considering the effect of a nonresonant $\chi^{(3)}$ process on the index of refraction of the nonresonant medium. In general, the effective refractive index is $n = n_0 + n_2(I)$,, where n_0 is a linear (zero-field) refractive index, n_2 is a parameter derived from the value of the nonresonant $\chi^{(3)}$, and I is the total light intensity. In the simulation with both pump and Stokes sources present, the effective refractive index is $n = n_0 + n_2(I_p + I_s)$, where I_p is the pump

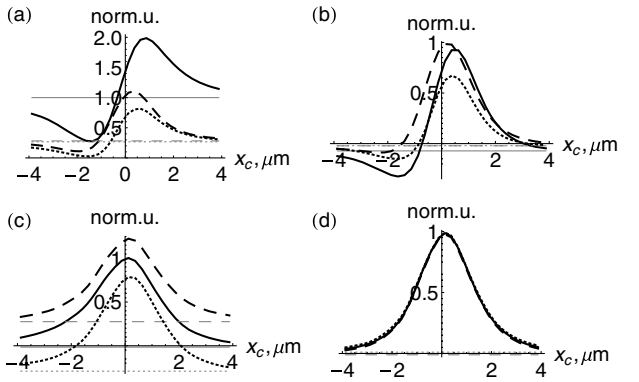

Fig. 2. FDTD simulations of the image formation process in coherent Raman scattering microscopies. Signal variation with bead position in the presence of a nonersonant background medium for (a) CARS; (b) FM-CARS; (c) AM-SRS; (d) FM-SRS. Solid lines: nonresonant background case 1; dashed lines: case 2; dotted lines: case 3. Signal level in the absence of the Raman bead is shown by thin lines. The "norm.u." stands for arbitrary normalized units.

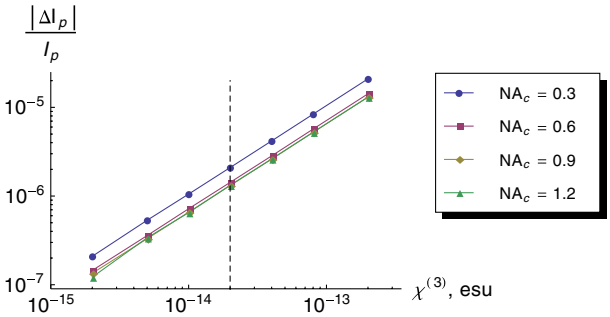

Fig. 3. (Color online) Parameter dependence of the nonresonant background signal in AM-SRS. Results of FDTD simulations with laser lens NA = 1.1. NA_c is the NA of the condenser lens. The magnitude of electronic $\chi^{(3)}$ of water is shown by the dashed line.

intensity and I_s the Stokes intensity. By contrast, in a simulation with the pump laser only, the refraction index is $n = n_0 + n_2 I_p$. Thus, the propagation of the pump pulse in the two scenarios is different.

In order to analyze these propagation effects, we have simulated the paraxial propagation of the pump pulse in a Kerr medium, using paraxial equation

$$2ik\frac{\partial E}{\partial x} + \Delta_\perp E + \frac{4\pi\omega^2}{c^2}\chi^{(3)}(x)E^3 = 0, \qquad (1)$$

where E is the complex field amplitude, ω the pump frequency, and k the wave vector length. We have solved Eq. (1) numerically with the boundary conditions corresponding to a Gaussian beam far from the focal plane. It was found that in the case of a uniform $\chi^{(3)}$ throughout the entire space the pump beam propagation is approximately symmetric about the focal plane, and the laser source divergence angle in the far field is almost independent on the magnitude of $\chi^{(3)}$. By contrast, if $\chi^{(3)} \neq 0$ only for, e.g., $x > 0$, the discontinuity in n_2 results in change of the divergence angle in the far field. If the condenser lens NA is lower than the laser lens NA, this change is detected as a background signal. When the condenser lens NA is higher than the laser lens NA, the background signal is still finite (Fig. 3). This is caused by the different reflection from the interface of the nonlinear medium in the experiments with Stokes on and Stokes off. Thus, in order for the AM-SRS to be background-free, it must be ensured that the entire energy of the scattered light is sent to the detector. This will require detection in the 4π solid angle. Otherwise, the sample-dependent nonlinear propagation effects will inevitably produce a nonresonant background.

Finally, we consider FM-SRS. Similar to FM-CARS, we measure the difference between the pump signals when the Stokes is on and off resonance. We again consider forward-collected signals. The results are shown in Fig. 2(d). The FM-SRS technique produces a largely background-free signal for both spatially homogeneous and heterogeneous nonresonant backgrounds.

This work was supported by the Natural Sciences and Engineering Research Council of Canada, Ontario Ministry of Research and Innovation, Canada Research Chairs program, Canada Foundation for Innovation and Mprime NCE Strategic Postdoctoral Research Program.

References

1. C. Evans and X. S. Xie, Annu. Rev. Anal. Chem. **1**, 883 (2008).
2. E. O. Potma and X. S. Xie, in *Handbook of Biological Nonlinear Optical Microscopy*, B. R. Masters and P. T. C. So, eds. (Oxford University, 2008), pp. 164–185.
3. B. G. Saar, C. W. Freudiger, J. Reichman, C. M. Stanley, G. R. Holtom, and X. S. Xie, Science **330**, 1368 (2010).
4. W. Min, C. W. Freudiger, S. Lu, and X. S. Xie, Annu. Rev. Phys. Chem. **62**, 507 (2011).
5. K. I. Popov, A. F. Pegoraro, A. Stolow, and L. Ramunno, Opt. Express **19**, 5902 (2011).
6. J. Cheng, L. Book, and X. Xie, Opt. Lett. **26**, 1341 (2001).
7. M. Jurna, J. P. Korterik, C. Otto, J. L. Herek, and H. L. Offerhaus, Phys. Rev. Lett. **103**, 043905 (2009).
8. F. Ganikhanov, C. Evans, B. G. Saar, and X. S. Xie, Opt. Lett. **31**, 1872 (2006).
9. G. C. Bjorklund, Opt. Lett. **5**, 15 (1980).
10. C. W. Freudiger, W. Min, B. G. Saar, S. Lu, G. R. Holtom, C. He, J. C. Tsai, J. X. Kang, and X. S. Xie, Science **322**, 1857 (2008).
11. Y. Ozeki, F. Dake, S. Kajiyama, K. Fukui, and K. Itoh, Opt. Express **17**, 3651 (2009).
12. R. W. Boyd, in *Nonlinear Optics*, 2nd ed. (Academic Press, 2003), p. 194.
13. A. F. Pegoraro, A. Ridsdale, D. J. Moffatt, Y. Jia, J. P. Pezacki, and A. Stolow, Opt. Express **17**, 2984 (2009).